Kuwait Journal of Science 51 (2024) 100102

Contents lists available at ScienceDirect

Kuwait Journal of Science

journal homepage: www.sciencedirect.com/journal/kuwait-journal-of-science

Full Length Article

Biosynthesis of zinc oxide nanoparticles mediated by *Strobilanthes hamiltoniana*: Characterizations, and its biological applications

Jaya Gangwar [a,1], Balamuralikrishnan Balasubramanian [b,1], Akshay Pratap Singh [c], Arun Meyyazhagan [a], Manikantan Pappuswamy [a], Amer M. Alanazi [d], Kannan R.R. Rengasamy [e,**], Joseph Kadanthottu Sebastian [a,*]

[a] Department of Life Sciences, CHRIST (Deemed to be University), Bangalore, Karnataka, 560029, India
[b] Department of Food Science and Biotechnology, College of Life Science, Sejong University, Gwangjin-gu, Seoul, 05006, Republic of Korea
[c] Department of Materials Engineering, Indian Institute of Science, Bangalore, Karnataka, 560012, India
[d] Pharmaceutical Chemistry Department, College of Pharmacy, King Saud University, Riyadh, 11451, Saudi Arabia
[e] Centre of Excellence for Pharmaceutical Sciences, North-West University, Potchefstroom, 2520, South Africa

ARTICLE INFO

Keywords:
Strobilanthes hamiltoniana
Zinc oxide
Dye degradation
Anti-cancer
Anti-Microbial

ABSTRACT

Nanoparticles of Zinc oxide (ZnONPs), has a variety of applications such as antibacterial property, water treatment for pollutant removal, and as catalysts for organic reactions etc. and have been synthesized utilizing a variety of approaches, including green synthesis, chemical precipitation, sol–gel, hydrothermal synthesis, and microwave-assisted synthesis. In the present work, easy and economically viable ZnONPs were synthesized utilizing *Strobilanthes hamiltoniana* (SH) leaf extracts. Phytochemicals form *S. hamiltoniana* act as agents for reducing and capping the metal oxide ions. A range of analytical and microscopic techniques have been used to investigate the physical and chemical properties of ZnONPs. At 360 nm, green synthesized SH-ZnONPs showed robust UV–Vis absorption. The nanosize, shape, and crystalline structure of SH-ZnO NPs were characterized using XRD and electron microscopy techniques. Using SH-ZnO NPs, the photocatalytic activity of textile dyes such as Reactive blue 220 (RB-220), Reactive blue 222A (RB-222A), Reactive yellow 145 (RY-145) and Reactive yellow 86 (RY-86) dyes showed degradation efficiency of 97.3%, 78.57%, 88.88%, and 83.33% after 320 min. ZnONPs exhibited remarkable antibacterial effectiveness against bacterial and fungal pathogens using the Minimum inhibitory concentration approach. Their MIC values were calculated, and free radical scavenging experiments showed antioxidant activity. The SH-ZnONPs were validated using HepG2 (IC50) cancerous cells lines and showed promising anti-cancer activity. These results revealed that SH-ZnO NPs had promising benefits that could be utilized as a viable therapeutic candidate.

Introduction

Nanotechnology is today regarded as a proven innovative technology with extensive applications in pharmaceutical, textile industries, wastewater treatment, drug delivery, mechanical, and food processing sectors (Khan et al., 2022; Shah et al., 2022). Due of their toxicity, NPs produced using conventional methods are only occasionally used therapeutically. This methodology also has the advantage of extending the life of the NPs due to the physio-chemical characteristics of plant-derived NPs, which avoids the drawbacks of traditional methods for synthesizing nanoparticles (Naseer et al., 2020). The use of plants in the green synthesis of ZnONPs has various advantages such as sustainable and ecologically friendly method that relies on natural resources rather than toxic chemicals. Plant extracts serve as widely accessible reducing and stabilising agents, making the procedure cost-effective. Plant-mediated synthesis also enables the synthesis of nanoparticles with regulated size, shape, and surface characteristics (Mutukwa et al., 2022). The functional groups in plant metabolites, interact with metallic ions to decrease to the nanoscale range (Marslin et al., 2018). Different plants have different phytochemical compositions, resulting in differences in nanoparticle properties. *Aloe vera* extracts, for example, can yield ZnONPs with increased UV-blocking features (Rasli et al., 2020), whereas neem

* Corresponding author.
** Corresponding author.
E-mail addresses: ragupathi.rengasamy@nwu.ac.za (K.R.R. Rengasamy), joseph.ks@christuniversity.in (J. Kadanthottu Sebastian).
[1] Equal contributed as first author.

https://doi.org/10.1016/j.kjs.2023.07.008
Received 17 April 2023; Received in revised form 29 June 2023; Accepted 23 July 2023

extracts and *Allium sativum* Extract provide nanoparticles with significant antibacterial activity (Sohail et al., 2020; Majeed et al., 2022). ZnONPs with antioxidant properties are produced by plants such as green tea (Irshad et al., 2018) and mustard (Geremew et al., 2023). Zinc oxide nanoparticles (ZnO NPs) have been biosynthesized in research using numerous medicinal plants (Gangwar and Sebastian, 2021). In the photocatalytic degradation of textile dyes utilizing green synthesized ZnONPs generated from plants, the ZnONPs absorb UV light, creating electron–hole pairs. These pairs are involved in redox processes that produce reactive oxygen species (ROS) such as hydroxyl radicals (•OH) (Shah et al., 2018). These •OH radicals are very reactive and play an vital role in dye degradation by breaking down the bonds between molecules through oxidation reactions (Iqbal et al., 2020).

S. hamiltoniana, commonly known as the Chinese Rain Bell, which belongs to the Acanthaceae family. The leaves of *S. hamiltoniana* contain bioactive compounds such as flavonoids, polyphenols, terpenoids, phenolic compounds and phytosterols. These extracts have biological properties such as anti-bacterial, antioxidant antifungal, antioxidant, anti-cancer and anthelmintic properties (Bennett and Scotland, 2003).

In the current study, we are using zinc acetate as a biological precursor for ZnO NPs and *S. hamiltoniana* leaf extract as a capping agent, we have developed a simple and environmentally benign method for producing ZnO NPs. The catalytic ability of biosynthesized nanoparticles to degrade azo dyes [Reactive Blue 220 (RB-220), Reactive Blue 222A (RB-222A), Reactive Yellow 145 (RY-145), and Reactive Yellow 86 (RY-86)] has been demonstrated. Nanoparticles' anti-bacterial and antifungal efficacy against four pathogens was investigated using the Minimum inhibitory concentration (MIC) technique. To assess the antioxidant effect, the 2,2-diphenyl-1-picrylhydrazyl (DPPH) assay was adopted. The HEP-G2 colon cancer cell line was utilized to evaluate the in vitro anticancer effects of biosynthesized nanoparticles using the MTT assay.

Materials and methods

Materials

Zinc acetate dihydrate, Nutrient Broth (NB), and Potato Dextrose Broth (PDB) were obtained from HiMedia Laboratories, India. DPPH, Ascorbic acid a (AA) and Methanol were procured from Merck chemicals, India. RB-220, RB-222A, RY-145, and RY-86 were obtained from Jetpur, India. The bacterial strains *Bacillus subtilis* (ATCC 6633), *Escherichia coli* (ATCC 10536), *Candida tropicalis* (ATCC 10231), and *Candida albicans* (ATCC 90028) were acquired from the Microbial Type Culture Collection and Gene Bank (MTCC). HEP-G2 cancer cell lines obtained from NCCS (Pune). Fresh *S. hamiltoniana* (SH) leaves were collected from FRLHT in Bangalore (13.1234° N, 77.5483° E), India and maintained in a greenhouse.

Plant extract preparation and biosynthesis of ZnONPs

Biosynthesis of SH-ZnO NPs is depicted in Fig. 1. 10 g of coarsely chopped and powdered leaves were measured and stirred for 20 min on a mechanical stirring at 60 °C in 100 mL of distilled water. Before filtering using Whatmann filter Paper No. 1, the solution was cooled. 1 mL of freshly prepared *S. hamiltoniana* leaves extract was mixed with 50 mL of 0.1M Zinc acetate solution at RT for 10 min with vigorous stirring (pH 10). The suspension was then held at 60 °C for 1 h with vigorous stirring (400 rpm) to develop a white colour. The synthesized nanoparticle was calcined at 500 °C for 2 h in a muffle furnace to form white SH-ZnO NPs. Chelation has been suggested as a potential method for reducing the acetate group of metal salts because of polyphenols (Naseer et al., 2018). Metal oxide NPs are formed during the calcination process when the interaction between the metal salt and the –OH group breakdowns, resulting in the loss of a water molecule (Kaur et al., 2018).

Characterization of the SH-ZnO NPs

The biosynthesized SH-ZnO NPS were detected using a UV–vis spectrophotometer (UV-1800, Shimadzu, Japan). FESEM was used to determine the structural properties of SH-ZnO NPs, such as crystalline structure and size (Gemini SEM 450, Carl Zeiss, Germany), TEM (JEM-2100F, JEOL, Slovak republic) has a significantly better resolution to understand particle size and shape, and XRD (Miniflex, Rigaku, Japan). The crystalline structure was determined using X-ray diffractions at 2 theta values obtained at 20–80° using Cu k radiations with a wavelength of 1.541 A°, and size was calculated using the XRD data using the Debye–Scherrer formula. For determining the size of NPs from FESEM, Image J software (version 1.53k) was used. For determining high-resolution (HR) TEM and selected-area electron diffraction (SAED) pattern examination were performed with the help of Digital Micrograph software. Using FTIR (IR spirit -L, Shimadzu, Japan) and an IR spectrophotometer, the functions of the biosynthesized SH-ZnO NPS and leaf extracts were investigated (IR spirt with single reflectance). Origin Pro 9.4 was used to construct the graphs.

Photocatalytic activity

For photocatalytic degradation analysis, in distilled water, 1 mg/mL of SH-ZnO NPs was dissolved and combined with 5 ppm of RB-220, RB-222A, RY-145 and RY-86, respectively. For 10–15 min, the mixture was kept in the dark (dark–adsorption equilibrium stage). UV light was later added in a photoreactor. Using a UV–vis spectrophotometer, absorbance at 200–800 nm was measured at regular time intervals (0–320 min). UV light was then supplied in a photoreactor. Absorbance at 200–800 nm was measured at regular time intervals (0–320 min). The photocatalytic degradation efficiency of SH-ZnO NPs was calculated using the given equation (Meena et al., 2016).

$$\% \ degradation = (A_0/A_t)/A_t \times 100$$

where A_o and A_t, respectively, denote time-dependent dye concentrations.

Phytotoxicity studies

The effectiveness of the dyes' degradation and toxicity decrease were assessed via. *Vigna radiata* toxicity and brine shrimp mortality tests. To

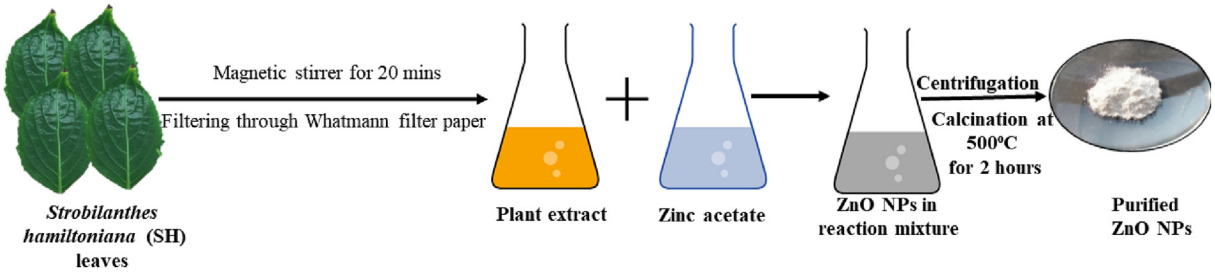

Fig. 1. Biosynthesis of green synthesized SH-ZnONPs.

examine *V. radiata* toxicity, seeds were sprouted with minor alterations. The seedlings were grown in petridishes (10 seeds each, 1 cm gap between seeds), then exposed to solutions containing treated and untreated dye as well as SH-ZnO NPs. After 7 days of treatment, the toxicity of the seedlings was determined together with their shoot and root lengths (Dharshini et al., 2021).

% germination = (Seeds germinated at final count/ seeds placed for germination)×100

The lethality assay for brine shrimp (*Artemia salina*) as previously described (Bilal et al., 2016) with minor modifications. Hatched eggs in artificial seawater (consist 36 g of non-iodized salt in 1l of deionized water). 10 nauplii were grown for 24 h at RT with treated and control dye, as well as NPs solutions. By counting the dead nauplii with a binocular microscope and applying the equation, the mortality rate (MR) was determined.

% mortality = (No. of dead nauplii/ Initial alive nauplii) × 100

MIC assay

SH-ZnO NPs MIC was calculated using a standard procedure developed by the Clinical and Laboratory Standards Institute (CLSI). The obtained cells were placed in a 10 mL with NB and PDB in test tube, and overnight (37 °C) cultured in an orbital shaker (120 rpm). The test bacterial and fungal cultures were pre-grown for 24 h at 37 °C using NB and PDB, as previously mentioned. In a 48-well microtiter plate containing NB and PDB, the SH-ZnO NPs were combined with sterile distilled water (stock concentration: 10 mg/mL) and diluted to obtain final concentrations ranging from 10 to 300 g/mL. A 24 h incubation period at 37 °C was followed by the inoculation of 0.5 mL of a bacterial and fungal solution (1x10^5 cells mL^{-1}). The MIC value was established as previously described (Ruparelia et al., 2008).

Antioxidant activity

In brief, the DPPH assay was used to examine SH-ZnO NPs. For this, various concentrations of nanoparticle and BHA (10–100 g/mL) were produced in 99% methanol. The solution of DPPH (0.004%) was then added and incubated (30 min) in dark. At 517 nm, a colour shift was noticed by means of a UV–Vis spectrophotometer. When scavenged, the DPPH becomes yellow instead of purple. As a control, 3 mL of DPPH was utilized (Adebiyi et al., 2017). The following equation is used to express radical scavenging activity:

$$Percentage\ of\ activity\ (\%) = \left(\frac{Absorbance_{control} - Absorbance_{sample}}{Absorbance_{control}}\right) \times 100$$

MTT assay using HEP-G2 cell lines

Trypsinization of the monolayer grown cells was carried out using matching medium containing 10% FBS, and the cell density was subsequently raised to 1.0 x 10^5 cells/mL. 100 l of the cell suspension (50,000 cells/well) was put to each well of the 96-well microtiter plate. Once a partial monolayer had formed after 24 h, the supernatant was flicked off, the monolayer had been washed with medium once, and 100 l of various test drug dosages had been put to the partial monolayer on microtiter plates. The plates were then incubated for a further 24 h at 37 °C with 5% CO_2. The test solutions removed after incubation, and 100 l of MTT (5 mg/10 mL MTT in PBS) was added to each well. The plates were incubated (5% CO_2 atmosphere) for 4 h at 37 °C. The plates were gently shaken to dissolve the formazan that had formed after 100 l of DMSO was added. The absorbance was measured (590 nm)using a microplate reader (Wahab et al., 2014). The dose–response curves for each cell line were used to determine the test substance concentration required to inhibit cell growth by 50% using the following method for calculating the percentage of growth inhibition (IC 50). This is a representation of the percentage of inhibition formula:

$$Percentage\ of\ inhibition\ (\%) = 100 - \left(\frac{OD\ of\ the\ sample}{OD\ of\ the\ Control}\right) \times 100$$

Results and discussion

Characterization of SH-ZnO NPs

Metal oxide nanoparticles' UV–Vis absorption spectra exhibited surface plasmon resonance (SPR) properties. The reaction mixture's colour altered during the synthesis process, suggesting the formation of metal oxide nanoparticles (Sangeetha et al., 2011). The spectrum of the solution was detected at 200–800 nm and exhibited a distinct absorption maxima peak at 360 nm (Fig. 2 A). The band gap energy of SH-ZnO NPs was 3.25 eV using Wood- Tauc's relation, with a peak intensity indicating nanometer-size particles with a narrow distribution (Kumar et al., 2016). The band energy was also reported to be lower than that of bulk ZnO. (3.45 eV). The SH-ZnO NPs' extensive diffraction peaks demonstrate that they are crystalline which ranges from 20º-80º. The recorded diffraction peaks at two different angles of 31.76°, 34.44°, 36.22°, 47.54°, 56.54°, 62.8°, 66.29°, 67.92°, and 69.08°, corresponding to the phases [100], [002] [101], [102] [110], [103] [020], [112], and [201] (Shamhari et al., 2018) (Fig. 2 B). The size of SH-ZnO NPs is correlated with the more prominent peak at 36.22°. The NPs average crystal size, calculated using the Debye–Scherrer formula, was determined to be 26.9 nm. The peaks corresponded to JCPDS number 98-001-1316 (Przybylska and Grzyb, 2020). According to a previously published study, SH-ZnO NPs displayed a hexagonal shape with lattice specifications of a = b = 3.2430 A° and c = 5.1950 Aº. Diverse IR spectra ranged between 400 and 4000

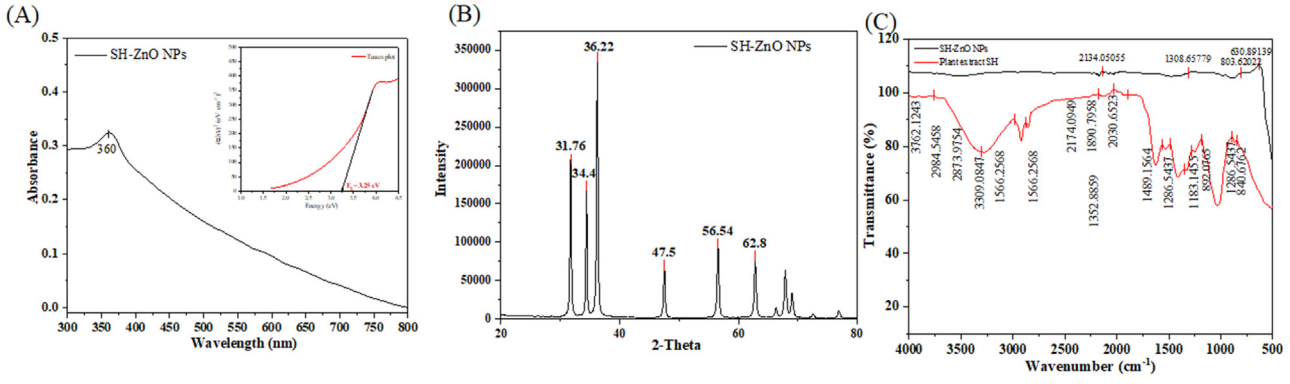

Fig. 2. UV visible spectroscopy, XRD and FTIR analysis of ZnONPs (**A**) UV (**B**) XRD (**C**) FTIR.

cm^{-1}, which facilitated synthesis of SH-ZnONPs by acting as reducing and capping agents, were evidence of the existence of unique functional groups of bioactive molecules bound on the surface of nanoparticles (Fig. 2C) (Farooq et al., 2022). Various studies suggest, the IR peaks between 470 and 800 cm^{-1} are caused by Zn–O stretching vibrations. Zn–O stretching vibrations reach their maximum at 630.89 cm^{-1}. A peak at 1489.15 cm^{-1} corresponds to "C═C," peaks at 2984.54, 2873.97, 2174.09, and 2030.65 cm^{-1} are related to C–H and C -C stretching vibrations, and peaks at 3762.12 and 33.9.08 cm^{-1} are related to alcohols and phenols of OH stretching, in accordance with the plant extract. These bands represent the presence of numerous phytochemicals found in earlier investigations, such as flavonoids, terpenoids, and phytosterols (S. et al., 2017).

The FE-SEM images taken at various magnifications (500 nm and 200 nm) revealed the shape and dimensions of SH-ZnO NPs (Fig. 3A). Highly scattered NPs and rods are visible. The ZnO NPs exhibited aggregation in the micrograph, which has been attributed to electrostatic attraction, synergistic activity, surface shape, nanoparticle polarity, and other factors that have been shown in previous reports (Geetha et al., 2016). The average length and thickness for SH-ZnO NPs was 403.5 nm and 76.83 nm respectively. The EDX was used for confirming the atomic content and elemental composition. The biosynthesis of pure SH-ZnONPs was corroborated by the high peak in the EDX spectra of the SH-ZnONPs (Fig. 3B). Except from 'Zn' and 'O,' no other peaks belonging to other elements were found, proving the crystalline phase purity of SH-ZnONPs (Fakhari et al., 2019).

The ZnO TEM imaging showed at different magnifications (500 nm and 200 nm), rod-shaped particles with little fluctuation in thickness, which is consistent with the FESEM data. This image demonstrates that the majority of the ZnO NPs are rods in form, with typical particle sizes of length and thickness 235.60 nm and 78.76 nm respectively (Fig. 4A and B) (M. et al., 2020). The SAED pattern showed that the diffraction rings of the biosynthesized ZnO exhibited lattice spacing of 0.327 nm and Debye Scherrer values of (002), (010) (012), and (013), respectively (Fig. 4C, D). The particle size measured by TEM is similar to that found by XRD pattern (Sali et al., 2021).

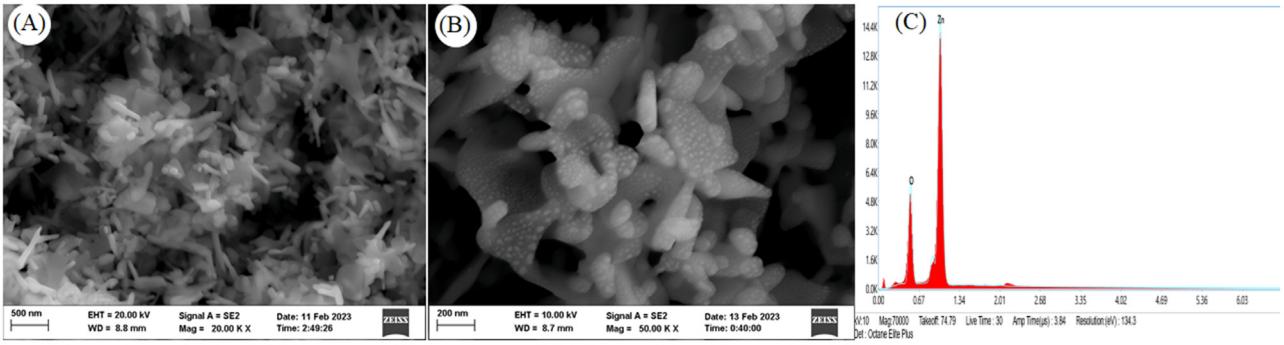

Fig. 3. FESEM and EDX analysis of biosynthesized SH-ZnONPs at different magnifications (A) SEM image at 500 nm magnification (B) SEM image at 200 nm magnification (C) EDX.

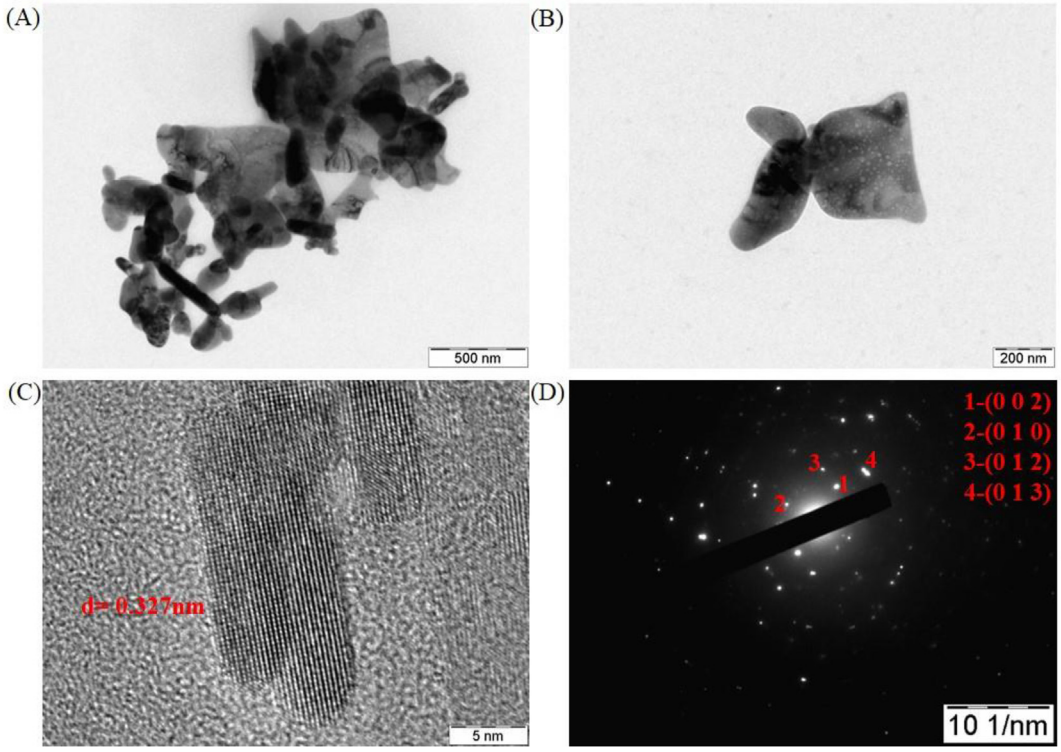

Fig. 4. HR-TEM and SAED analysis of green synthesized SH-ZnONPs. (A) HR-TEM image of ZnO nanoparticles (B) The individual particles (lattice image) (D)The selected area electron diffraction (SAED) pattern.

The degrading effectiveness of SH-ZnO NPs was assessed under UV irradiation using the dyes. Additionally, the UV–vis spectra of the reaction mixture at 665 nm, 598 nm, 420 nm, and 408 nm for RB-220, RB-222A, RY-86, and RY-145, respectively, determined the photodegradation of dyes. Fig. 5 A-D depicted the time-dependent degradation of the dyes RB-220, RB-222A, RY-86, and RY-145. The absorbance of dyes reduced with an increase in concentration from 0 to 320 min, revealing a gradual reduction in dye concentration and degradation efficiency of 97.3%, 78.57%, 88.88%, and 83.33% after 320 min, respectively. The ZnONPs absorb UV light, creating electron–hole pairs. These pairs are involved in redox processes that produce reactive oxygen species (ROS) such as hydroxyl radicals (•OH) (Shah et al., 2018). When higher radiation energies than band gap energy strike the catalyst surface, photochemical reactions may arise from the creation of holes (h+) in the valence band and electrons (e−) in the conduction band (Fig. 6). Reactive oxygen species (ROS), which can cause the deterioration of dyes, can be produced when the h + oxidizes H_2O to produce OH radicals. ROS include hydroxyl radicals (OH), superoxide ions (O_2), and others (Spitaleri et al., 2019). These •OH radicals are very reactive and play an important role in textile dye degradation by breaking down the bonds between molecules through oxidation reactions. He et al. (2014) identified superoxide radicals (•O2), hydroxyl radicals (•OH), and holes (h+) as the primary radicals generated during UV irradiation of ZnO nanoparticles using electron spin resonance spectroscopy. Superoxide radicals directly destroy dyes, hydroxyl radicals have significant oxidation capabilities and breakdown dye molecules, and electron holes engage in oxidation processes by withdrawing electrons from the dyes (He et al., 2014).

Briefly, degradation has been done using UV-light as it excites the movement of electrons from to valence to conduction band, the energy received can cause chemical methods that break down the dye molecules into smaller, less coloured, or non-colored compounds. The experimental setup is at lab-scale conditions with efficient degradation of textile dyes. Further it has to be tested at industrial-scale which can be combined with other methods such as advanced oxidation processes (AOP) for complete eradication of dye pollutants from wastewater (Peerakiatkhajohn et al., 2021).

The chemically synthesized ZnONPs have UV–visible spectral analysis wavelength range of 370–385 nm, a size range of 10–50 nm, and diverse morphologies such as spherical, rod-like, or hexagonal forms. The Wurtzite crystal structure is typical of ZnONPs. The (100), (002) (101), and (110) planes of ZnO are widely recognized in XRD peaks. ZnONPs bandgap energies are generally in the 3.2–3.4 eV range. Chemically synthesized NPs demonstrated the highest percentage decolorization of Rubine-GDB and Congo red with 89.058%, 88.888% after 96 h (Swain et al., 2021). In the present study we have obtained similar results with absorption maxima peak as 360 nm. According to our results we have obtained rods shaped structure which was confirmed by SEM and TEM. The XRD of SH-ZnO NPs was similar to chemically synthesized NPs. We have approached green synthesis route for biosynthesis of ZnONPs which

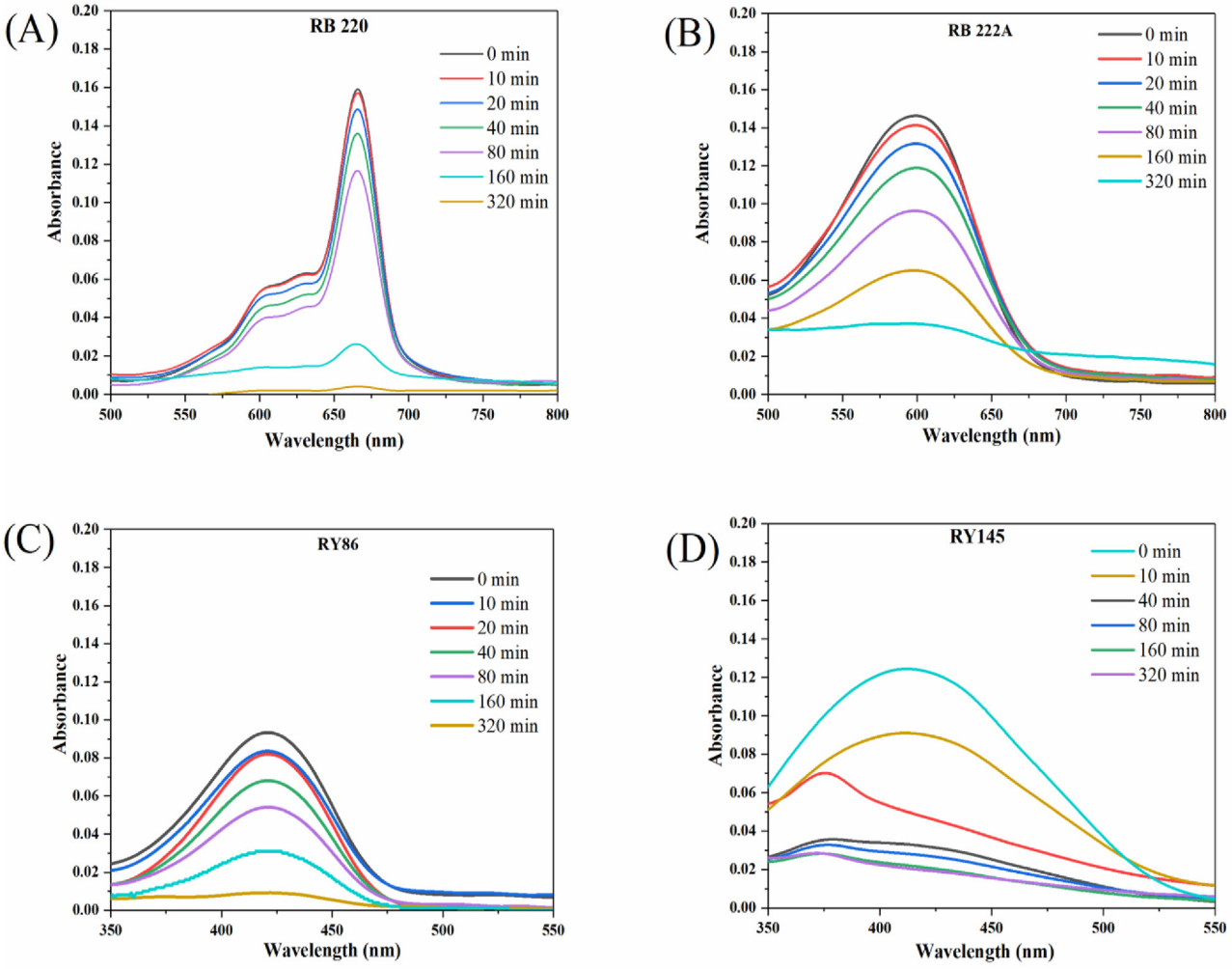

Fig. 5. Photo-catalytic degradation of dyes in time-dependent manner form 0 min to 320 min (A) RB-220 (B) RB-222A (C) RY-86 (D) RY-145.

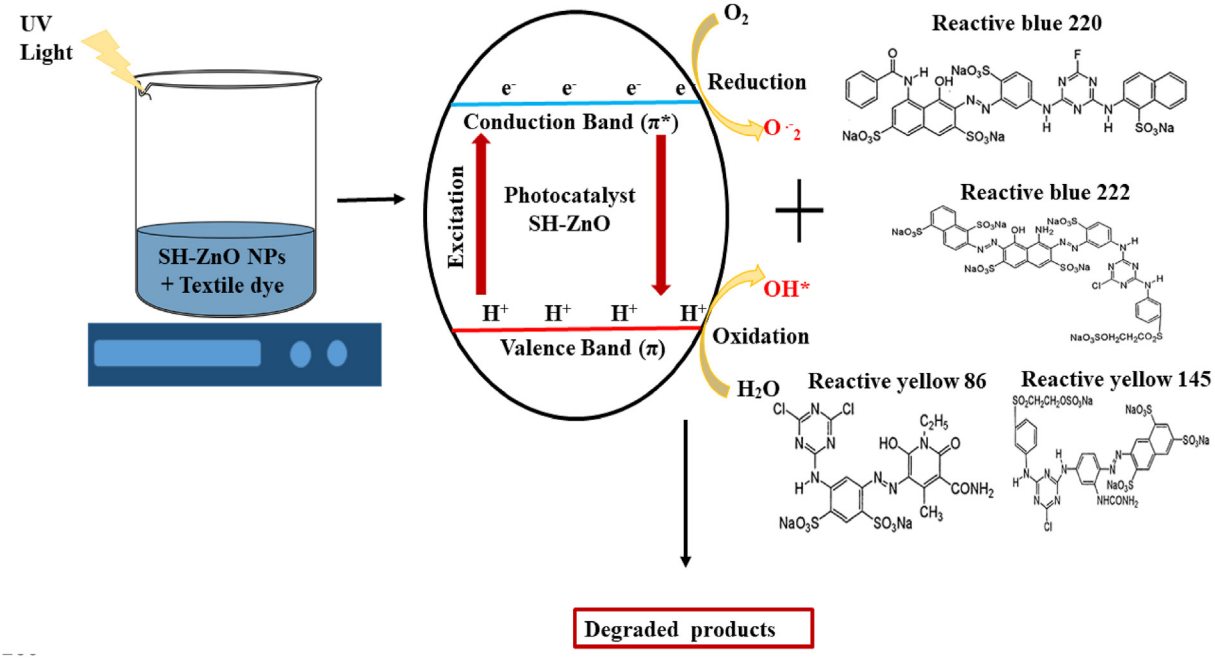

Fig. 6. Schematic representation of possible mechanism involved in photodegradation of dyes using green synthesized SH-ZnONPs.

includes numerous advantages over chemically synthesized ZnONPs including being environmentally friendly, cost-effectiveness, safety, sustainability, and increased bioactivity. It eliminates the use of hazardous chemicals, makes use of easily available and inexpensive plant resources. The nanoparticles synthesized are biocompatible and non-toxic, making them appropriate for a variety of applications. The inclusion of bioactive chemicals in plant extracts increases the bioactivity of ZnONPs, allowing for prospective applications in antibacterial, antioxidant, and anticancer sectors. Overall, green synthesis using plants is a safe, sustainable, and efficient way of synthesizing ZnONPs.

Phytotoxic studies

Toxicity tests were performed on both the untreated and treated dyes. The phytotoxicity of the treated and untreated dyes is summarized in Table 1. In seeds from *V. radiata*, the percentage of dyes that were inhibited by SH-ZnO NPs was significantly reduced. Previous research has shown that ZnO NPs are effective at reducing seed germination inhibition (Modi et al., 2022). Since they are essential to the aquatic life cycle, *Artemia* is an essential model for bioassay and toxicity. According to an *Artemia* toxicity assay, the elimination of harmful effects from industrial dye-contaminated waters is accomplished very well by SH-ZnO NPs treatment on dyes (Ozkan et al., 2016). According to reports, ZnO NPs are not hazardous to *Artemia* species and can thus be utilized in water bodies to remediate industrial effluents (Ravichandran et al., 2020).

Antimicrobial studies using minimum inhibitory concentration (MIC) method

Two bacterial strains (*B. subtilis* and *E. coli*) were tested for the capacity of SH-ZnO NPs to inhibit growth at dosages ranging from 20 to 100 g/mL. The SH-ZnO NPs showed IC_{90} for *E.coli* was 40.75 µg/mL and for *B. subtilis* was 41.48 µg/mL. To validate antifungal capacity, SH-ZnO NPs were tested against *C. tropicalis* (ATCC 10231) and *C. albicans* at 20–100 µg/mL doses. The SH-ZnO NPs showed IC_{90} for *C. tropicalis* was 40.40 µg/mL and for *C. albicans* was 39.54 µg/mL (Table 2). The phytochemicals coated onto the surface of nanomaterials may be responsible for ZnONPs significant bactericidal capability. Moreover, investigations have shown that the bactericidal and fungicidal effects of ZnONPs may be brought on by ROS induced by microbial cell-membrane pores or other mechanisms. Besides this, these nanoparticles have microscopic holes that allow for easy entry into microbial cell membranes. These pores might lead to mineral imbalances and the leakage of internal proteins and enzymes, which would eventually halt cell growth and result in cell

Table 1
Toxicity studies.

Sl.No.	Characters and treatment	*Vigna radiata* toxicity			Brine shrimp mortality		
		Germination percentage (%)	Average stem toxicity (%)	Average root toxicity (%)	Average Initial number of live nauplii	Average number of dead nauplii	Percentage mortality (%)
1	Distilled water	100	0	0	10.0 ± 0	0.33 ± 0.58	3.33
2	Negative control (Potassium permanganate solution)	–	–	–	10.0 ± 0	9.67 ± 0.58	96.67
3	RB 220	10	68 ± 0	75 ± 0.57	10.3 ± 0.58	7.67 ± 0.58	74.19
4	RB 222	12	70 ± 0.57	80.4 ± 0.57	10.0 ± 0	6.67 ± 0.58	66.67
5	RY 86	15	63.2 ± 0.57	82.9 ± 0.28	10.0 ± 0	6.33 ± 0.58	63.33
6	RY 145	13	73.36 ± 0.57	70.57 ± 1	10.0 ± 0	6.33 ± 0.58	63.33
7	SH-ZnO NPs	90	20 ± 3.2	40 ± 1.5	10.3 ± 0.58	1.67 ± 0.58	16.13
8	T- RB 220	95	9.6 ± 1.15	41.34 ± 0	10.3 ± 0.58	1.00 ± 1	9.68
9	T-RB 222	90	4 ± 1.73	26.68 ± 0	10.3 ± 0.58	1.00 ± 1	9.68
10	T-RY 86	92	4 ± 0.57	7.62 ± 0.57	10.3 ± 0.58	1.67 ± 0.58	2.00
11	T-RY 145	95	25.6 ± 0.5	1.75 ± 0	10.7 ± 1.15	0.33 ± 0.58	3.13

Table 2
Antimicrobial property using Minimum inhibitory concentration (MIC) method.

Strains		IC_{90} (μg/ml)	MIC (μg/ml)	Percentage of inhibition at MIC (%)
Bacterial strains	*E. coli* (ATCC 10536)	40.75	100	95.36
	B. subtilis (ATCC 6633)	41.48	100	95.83
Fungal strains	*C. tropicalis* (ATCC 10231)	40.4	100	96.13
	C. albicans (ATCC 90028)	39.54	100	96.69

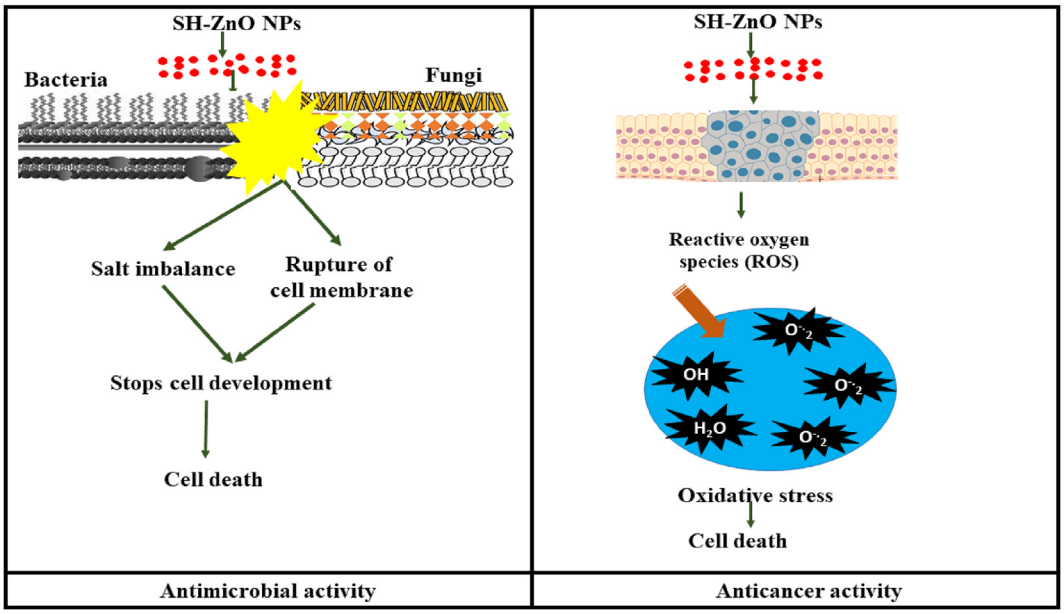

Fig. 7. Diagrammatic representation of possible mechanism involved for antimicrobial and anticancer properties.

death (Ozkan et al., 2016; Ravichandran et al., 2020; Sirelkhatim et al., 2015) (Fig. 7).

Antioxidant activity

The DPPH test was employed for evaluating the antioxidant property of the SH-ZnONPs. The stable DPPH radical shifts to yellow with a decrease in absorbance following reduction and exhibits a maximal red colour at 517 nm (Nethravathi et al., 2015) (Table 3). This makes it clear that the samples' antioxidant activity is dose-dependent. At higher concentrations of 100 μg/mL, SH-ZnONPs (50.81%) demonstrated the greatest percentage of inhibition against AA (97.22%) as a standard. The inhibitory effect is defined as the minimal sample concentration required to lower absorbance to half that of the positive control (IC50). The results showed that 72.99 g/mL was the IC50 value for SH-ZnO NPs (Khan et al., 2018).

MTT assay using HEP-G2 cell lines

The anti-cancer activities of SH-ZnONPs were investigated using MTT assays against liver cancer cell lines (HEP-G2). A concentration-dependent response was detected when cancer cell lines were treated to varied dosages of SH-ZnONPs (10–100 μM). The IC50 values for SH-ZnONPs were measured to be 46.25 ± 0.05 M. Many phytochemicals from leaf extracts that have been adsorbed onto the surface of ZnONPs, even at low concentrations, may be responsible for the anti-cancer effect (Hussin et al., 2015) (Fig. 8). In the HEP-G2 cell lines when exposed to SH-ZnO NPs, it was observed that cells were ruptured and distorted in shape whereas, in control the cells were intact and oval in shape (Siddiquah et al., 2018) (Fig. 9A and B). ZnONPs' capacity to function as semiconductors causes oxidative stress on tumour cells, which produces reactive oxygen species (ROS) and causes cell death (Bisht and Rayamajhi, 2016) (Fig. 7).

Table 3
Antioxidant property using DPPH assay.

Concentration (μg/mL)	Percentage of Scavenging activity (%)	IC_{50} (μg/mL)
10	47.928	72.99
20	48.468	
40	49.009	
60	49.550	
80	50.270	
100	50.811	

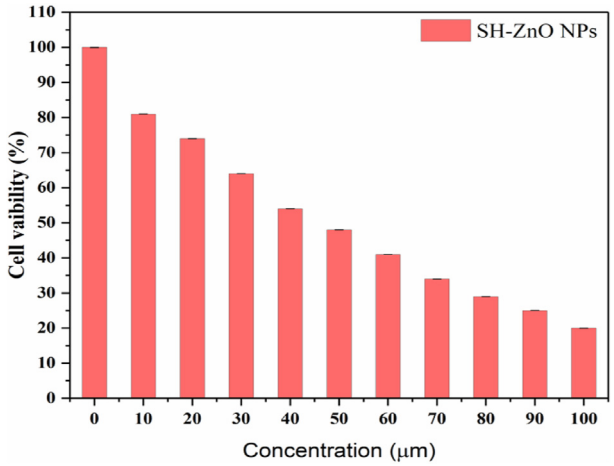

Fig. 8. Anticancer property of SH-ZnONPs.

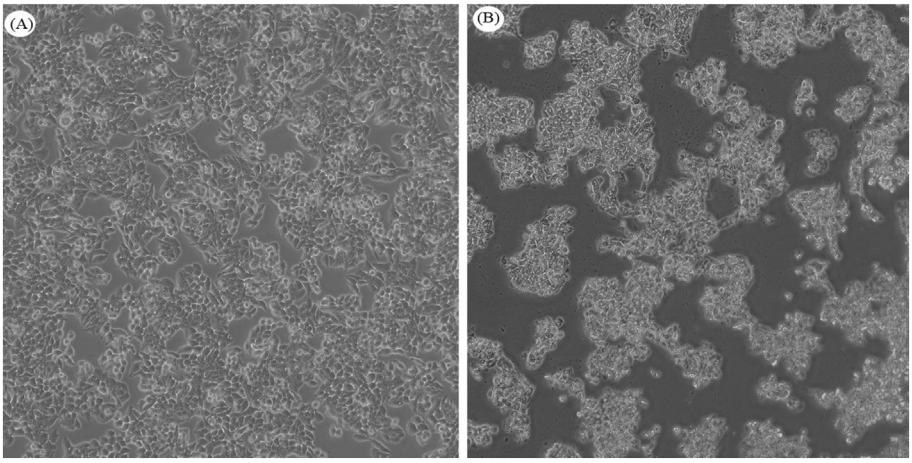

Fig. 9. HEP-G2 cell lines exposed to SH-ZnONPs (A) Control (B) Treated.

Conclusion and future prospects

In conclusion, our work established a straightforward and environmentally benign strategy for ZnONPs synthesis using a toxin-free and phytochemical-rich leaf extract from *S. hamiltoniana*. In UV–Vis spectral analysis, a distinctive peak at 360 nm was seen, and FTIR analysis was used to determine which biomolecules were present. XRD measurement revealed the crystalline characteristics of the synthesised ZnO-NPs. FESEM and TEM was used to validate the nanoparticles shape as rods wwith little flucuation. The degradation of textile dyes (RB-220, RB-222A, RY-86, and RY-145) was highest when the nanoparticles were exposed to UV light. A colon cancer cell line was significantly cytotoxic to the nanoparticles (HEP-G2) with IC_{50} concentration as 46.25 ± 0.05 M. Moreover, the nanoparticles have antioxidant and antibacterial properties. The breakdown of textile colours is effectively catalysed by the nanoparticles As a result, *S. hamiltoniana* leaf extract-derived ZnO nanoparticles can be used as effective anti-cancer, antioxidant, antibacterial, and catalytic agents.

To assess their nanopharmacological significance in various bioactivities such as biocompatibility and enzyme inhibition potential, further in vitro, in vivo, and mechanistic investigations using various animal models would be required in the future.

Author contributions

This research article was produced through collaboration between the authors. Conceptualization, J.K.S, K.R.R.R and B.B.; writing—original manuscript, J.G and B.B.; Methodology, data curation, and formal analysis, J.G., A.P.S., A.M., M.P.; Review and editing, B.B., A.M.A. and K.R.R.R.; Interpretation, and review/revision, A.M.A., K.R.R.R. and J.K.S. All authors have read and agreed to the published version of the manuscript.

Funding

This research received no external funding.

Institutional review board statement

Not applicable.

Informed consent statement

Not applicable.

Data availability statement

The data presented in this study are available on request from the corresponding authors.

Declaration of competing interest

The authors declare that they have no known competing financial interests or personal relationships that could have appeared to influence the work reported in this paper.

Acknowledgments

All the authors are thankful to their respective universities and institutes for their support and this work was funded by the Researchers Supporting Project Number (Project Number: RSP2023R261) King Saud University, Riyadh, Saudi Arabia.

References

Adebiyi, O.E., Olayemi, F.O., Ning-Hua, T., Guang-Zhi, Z., 2017. In vitro antioxidant activity, total phenolic and flavonoid contents of ethanol extract of stem and leaf of Grewia carpinifolia. Beni-Suef University Journal of Basic and Applied Sciences 6, 10–14. https://doi.org/10.1016/j.bjbas.2016.12.003.

Bennett, J.R., Scotland, R.W., 2003. A revision of Strobilanthes (Acanthaceae) in java. Kew Bull. 58, 1. https://doi.org/10.2307/4119356.

Bilal, M., Iqbal, M., Hu, H., Zhang, X., 2016. Mutagenicity, cytotoxicity and phytotoxicity evaluation of biodegraded textile effluent by fungal ligninolytic enzymes. Water Sci. Technol. 73, 2332–2344. https://doi.org/10.2166/wst.2016.082.

Bisht, G., Rayamajhi, S., 2016. ZnO nanoparticles: a promising anticancer agent. Nanobiomedicine 3, 9. https://doi.org/10.5772/63437.

Dharshini, R.S., Poonkothai, M., Srinivasan, P., Mythili, R., Syed, A., Elgorban, A.M., Selvankumar, T., Kim, W., 2021. Nano-decolorization of methylene blue by Phyllanthus reticulatus iron nanoparticles: an eco-friendly synthesis and its antimicrobial, phytotoxicity study. Appl. Nanosci. https://doi.org/10.1007/s13204-021-02002-3.

Fakhari, S., Jamzad, M., Kabiri Fard, H., 2019. Green synthesis of zinc oxide nanoparticles: a comparison. Green Chem. Lett. Rev. 12, 19–24. https://doi.org/10.1080/17518253.2018.1547925.

Farooq, A., Khan, U.A., Ali, H., Sathish, M., Naqvi, S.A.H., Iqbal, S., Ali, H., Mubeen, I., Amir, M.B., Mosa, W.F.A., Baazeem, A., Moustafa, M., Alrumman, S., Shati, A., Negm, S., 2022. Green chemistry based synthesis of zinc oxide nanoparticles using plant derivatives of calotropis gigantea (giant milkweed) and its biological applications against various bacterial and fungal pathogens. Microorganisms 10, 2195. https://doi.org/10.3390/microorganisms10112195.

Gangwar, J., Sebastian, J.K., 2021. Unlocking the potential of biosynthesized zinc oxide nanoparticles for degradation of synthetic organic dyes as wastewater pollutants. Water Sci. Technol. 84, 3286–3310. https://doi.org/10.2166/wst.2021.430.

Geetha, M.S., Nagabhushana, H., Shivananjaiah, H.N., 2016. Green mediated synthesis and characterization of ZnO nanoparticles using Euphorbia Jatropa latex as reducing agent. J. Sci.: Advanced Materials and Devices 1, 301–310. https://doi.org/10.1016/j.jsamd.2016.06.015.

Geremew, A., Carson, L., Woldesenbet, S., Wang, H., Reeves, S., Brooks, N., Saganti, P., Weerasooriya, A., Peace, E., 2023. Effect of zinc oxide nanoparticles synthesized from Carya illinoinensis leaf extract on growth and antioxidant properties of mustard (Brassica juncea). Front. Plant Sci. 14, 1108186. https://doi.org/10.3389/fpls.2023.1108186.

He, W., Zhao, H., Jia, H., Yin, J.-J., Zheng, Z., 2014. Determination of reactive oxygen species from ZnO micro-nano structures with shape-dependent photocatalytic activity. Mater. Res. Bull. 53, 246–250. https://doi.org/10.1016/j.materresbull.2014.02.020.

Hussin, F., Eshkoor, S.A., Rahmat, A., Othman, F., Akim, A., Eshak, Z., 2015. Strobilanthes crispus juice concentrations and anticancer effects on DNA damage, apoptosis and Gene expression in hepatocellular carcinoma cells. Asian Pac. J. Cancer Prev. APJCP 16, 6047–6053. https://doi.org/10.7314/APJCP.2015.16.14.6047.

Iqbal, J., Shah, N.S., Sayed, M., Ali Khan, J., Muhammad, N., Khan, Z.U.H., Saif-ur-Rehman, Naseem, M., Howari, F.M., Nazzal, Y., Niazi, N.K., Hussein, A., Polychronopoulou, K., 2020. Synthesis of nitrogen-doped Ceria nanoparticles in deep eutectic solvent for the degradation of sulfamethaxazole under solar irradiation and additional antibacterial activities. Chem. Eng. J. 394, 124869. https://doi.org/10.1016/j.cej.2020.124869.

Irshad, S., Salamat, A., Anjum, A.A., Sana, S., Saleem, R.S., Naheed, A., Iqbal, A., 2018. Green tea leaves mediated ZnO nanoparticles and its antimicrobial activity. Cogent Chemistry 4, 1469207. https://doi.org/10.1080/23312009.2018.1469207.

Kaur, S., Singh, J., Rawat, R., Kumar, S., Kaur, H., Venkateswara Rao, K., Rawat, M., 2018. A smart LPG sensor based on chemo-bio synthesized MgO nanostructure. J. Mater. Sci. Mater. Electron. 29, 11679–11687. https://doi.org/10.1007/s10854-018-9266-y.

Khan, Z.U.H., Khan, A., Chen, Y.M., Shah, N.S., Khan, A.U., Muhammad, N., Tahir, K., Shah, H.U., Khan, Z.U., Shakeel, M., Nadeem, M., Imran, M., Wan, P., 2018. Enhanced antimicrobial, anti-oxidant applications of green synthesized AgNPs- an acute chronic toxicity study of phenolic azo dyes & study of materials surface using X-ray photoelectron spectroscopy. J. Photochem. Photobiol. B Biol. 180, 208–217. https://doi.org/10.1016/j.jphotobiol.2018.02.015.

Khan, Y., Sadia, H., Ali Shah, S.Z., Khan, M.N., Shah, A.A., Ullah, N., Ullah, M.F., Bibi, H., Bafakeeh, O.T., Khedher, N.B., Eldin, S.M., Fadhl, B.M., Khan, M.I., 2022. Classification, synthetic, and characterization approaches to nanoparticles, and their applications in various fields of nanotechnology: a review. Catalysts 12, 1386. https://doi.org/10.3390/catal12111386.

Kumar, S., Singh, V., Tanwar, A., 2016. Structural, morphological, optical and photocatalytic properties of Ag-doped ZnO nanoparticles. J. Mater. Sci. Mater. Electron. 27, 2166–2173. https://doi.org/10.1007/s10854-015-4227-1.

M, S., H, N., V, P.P., 2020. In vitro biocompatibility and antimicrobial activities of zinc oxide nanoparticles (ZnO NPs) prepared by chemical and green synthetic route— a comparative study. BioNanoSci 10, 112–121. https://doi.org/10.1007/s12668-019-00698-w.

Majeed, S., Norshah, N.S.B., Danish, M., Ibrahim, M.N.M., Nanda, A., 2022. Biosynthesis of zinc oxide nanoparticles from Allium sativum extract: characterization and application. BioNanoSci 12, 795–803. https://doi.org/10.1007/s12668-022-01009-6.

Marslin, G., Siram, K., Maqbool, Q., Selvakesavan, R., Kruszka, D., Kachlicki, P., Franklin, G., 2018. Secondary metabolites in the green synthesis of metallic nanoparticles. Materials 11, 940. https://doi.org/10.3390/ma11060940.

Meena, S., Vaya, D., Das, B.K., 2016. Photocatalytic degradation of Malachite Green dye by modified ZnO nanomaterial. Bull. Mater. Sci. 39, 1735–1743. https://doi.org/10.1007/s12034-016-1318-4.

Modi, S., Yadav, V.K., Choudhary, N., Alswieleh, A.M., Sharma, A.K., Bhardwaj, A.K., Khan, S.H., Yadav, K.K., Cheon, J.-K., Jeon, B.-H., 2022. Onion peel waste mediated-green synthesis of zinc oxide nanoparticles and their phytotoxicity on mung bean and wheat plant growth. Materials 15, 2393. https://doi.org/10.3390/ma15072393.

Mutukwa, D., Taziwa, R., Khotseng, L.E., 2022. A review of the green synthesis of ZnO nanoparticles utilising southern african indigenous medicinal plants. Nanomaterials 12, 3456. https://doi.org/10.3390/nano12193456.

Naseer, S., Hussain, S., Naeem, N., Pervaiz, M., Rahman, M., 2018. The phytochemistry and medicinal value of Psidium guajava (guava). Clin Phytosci 4, 32. https://doi.org/10.1186/s40816-018-0093-8.

Naseer, M., Aslam, U., Khalid, B., Chen, B., 2020. Green route to synthesize Zinc Oxide Nanoparticles using leaf extracts of Cassia fistula and Melia azadarach and their antibacterial potential. Sci. Rep. 10, 9055. https://doi.org/10.1038/s41598-020-65949-3.

Nethravathi, P.C., Shruthi, G.S., Suresh, D., Udayabhanu, Nagabhushana, H., Sharma, S.C., 2015. Garcinia xanthochymus mediated green synthesis of ZnO nanoparticles: photoluminescence, photocatalytic and antioxidant activity studies. Ceram. Int. 41, 8680–8687. https://doi.org/10.1016/j.ceramint.2015.03.084.

Ozkan, Y., Altinok, I., Ilhan, H., Sokmen, M., 2016. Determination of TiO2 and AgTiO2 nanoparticles in Artemia salina: toxicity, morphological changes, uptake and depuration. Bull. Environ. Contam. Toxicol. 96, 36–42. https://doi.org/10.1007/s00128-015-1634-1.

Peerakiatkhajohn, P., Butburee, T., Sul, J.-H., Thaweesak, S., Yun, J.-H., 2021. Efficient and rapid photocatalytic degradation of methyl orange dye using Al/ZnO nanoparticles. Nanomaterials 11, 1059. https://doi.org/10.3390/nano11041059.

Przybylska, D., Grzyb, T., 2020. Synthesis and up-conversion of core/shell SrF2:Yb3+,Er3+@SrF2:Yb3+,Nd3+ nanoparticles under 808, 975, and 1532 nm excitation wavelengths. J. Alloys Compd. 831, 154797. https://doi.org/10.1016/j.jallcom.2020.154797.

Rasli, N.I., Basri, H., Harun, Z., 2020. Zinc oxide from aloe vera extract: two-level factorial screening of biosynthesis parameters. Heliyon 6, e03156. https://doi.org/10.1016/j.heliyon.2020.e03156.

Ravichandran, V., Sumitha, S., Ning, C.Y., Xian, O.Y., Kiew Yu, U., Paliwal, N., Shah, S.A.A., Tripathy, M., 2020. Durian waste mediated green synthesis of zinc oxide nanoparticles and evaluation of their antibacterial, antioxidant, cytotoxicity and photocatalytic activity. Green Chem. Lett. Rev. 13, 102–116. https://doi.org/10.1080/17518253.2020.1738562.

Ruparelia, J.P., Chatterjee, A.K., Duttagupta, S.P., Mukherji, S., 2008. Strain specificity in antimicrobial activity of silver and copper nanoparticles. Acta Biomater. 4, 707–716. https://doi.org/10.1016/j.actbio.2007.11.006.

Mahalakshmi, S., Hema, N., Vijaya, P.P., 2017. Antimicrobial and antioxidant potentials of biosynthesized colloidal zinc oxide nanoparticles for a fortified cold cream formulation: a potent nanocosmeceutical application. Mater. Sci. Eng. C 79, 581–589. https://doi.org/10.1016/j.msec.2017.05.059.

Sali, R.K., Pujar, M.S., Patil, S., Sidarai, A.H., 2021. Green synthesis of ZnO and Ag-ZnO nanoparticles using macrotyloma uniflorum: evaluation of antibacterial activity. Adv. Mater. Lett. 12, 1–7. https://doi.org/10.5185/amlett.2021.071645.

Sangeetha, G., Rajeshwari, S., Venckatesh, R., 2011. Green synthesis of zinc oxide nanoparticles by aloe barbadensis miller leaf extract: structure and optical properties. Mater. Res. Bull. 46, 2560–2566. https://doi.org/10.1016/j.materresbull.2011.07.046.

Shah, N.S., Khan, J.A., Sayed, M., Khan, Z.U.H., Rizwan, A.D., Muhammad, N., Boczkaj, G., Murtaza, B., Imran, M., Khan, H.M., Zaman, G., 2018. Solar light driven degradation of norfloxacin using as-synthesized Bi3+ and Fe2+ co-doped ZnO with the addition of HSO5−: toxicities and degradation pathways investigation. Chem. Eng. J. 351, 841–855. https://doi.org/10.1016/j.cej.2018.06.111.

Shah, N.S., Iqbal, J., Sayed, M., Ghfar, A.A., Khan, J.A., Khan, Z.U.H., Murtaza, B., Boczkaj, G., Jamil, F., 2022. Enhanced solar light photocatalytic performance of Fe-ZnO in the presence of H2O2, S2O82−, and HSO5− for degradation of chlorpyrifos from agricultural wastes: toxicities investigation. Chemosphere 287, 132331. https://doi.org/10.1016/j.chemosphere.2021.132331.

Shamhari, N.M., Wee, B.S., Chin, S.F., Kok, K.Y., 2018. Synthesis and characterization of zinc oxide nanoparticles with small particle size distribution. ACSi 65, 578–585. https://doi.org/10.17344/acsi.2018.4213.

Siddiquah, A., Hashmi, S.S., Mushtaq, S., Renouard, S., Blondeau, J.P., Abbasi, R., Hano, C., Abbasi, B.H., 2018. Exploiting in vitro potential and characterization of surface modified zinc oxide nanoparticles of Isodon rugosus extract: their clinical potential towards HepG2 cell line and human pathogenic bacteria. EXCLI Journal 17 (Doc671). https://doi.org/10.17179/EXCLI2018-1327. ISSN 1611-2156.

Sirelkhatim, A., Mahmud, S., Seeni, A., Kaus, N.H.M., Ann, L.C., Bakhori, S.K.M., Hasan, H., Mohamad, D., 2015. Review on zinc oxide nanoparticles: antibacterial activity and toxicity mechanism. Nano-Micro Lett. 7, 219–242. https://doi.org/10.1007/s40820-015-0040-x.

Sohail, M.F., Rehman, M., Hussain, S.Z., Huma, Z., Shahnaz, G., Qureshi, O.S., Khalid, Q., Mirza, S., Hussain, I., Webster, T.J., 2020. Green synthesis of zinc oxide nanoparticles by Neem extract as multi-facet therapeutic agents. J. Drug Deliv. Sci. Technol. 59, 101911. https://doi.org/10.1016/j.jddst.2020.101911.

Spitaleri, L., Nicotra, G., Zimbone, M., Contino, A., Maccarrone, G., Alberti, A., Gulino, A., 2019. Fast and efficient sun light photocatalytic activity of Au_ZnO core–shell nanoparticles prepared by a one-pot synthesis. ACS Omega 4, 15061–15066. https://doi.org/10.1021/acsomega.9b01850.

Swain, J., Kulkarni, P., Manuel, S., 2021. Decolorization of azodyes by chemically and biosynthesized ZnO nanoparticles. Rev. https://doi.org/10.21203/rs.3.rs-722394/v1.

Wahab, R., Siddiqui, M.A., Saquib, Q., Dwivedi, S., Ahmad, J., Musarrat, J., Al-Khedhairy, A.A., Shin, H.-S., 2014. ZnO nanoparticles induced oxidative stress and apoptosis in HepG2 and MCF-7 cancer cells and their antibacterial activity. Colloids Surf. B Biointerfaces 117, 267–276. https://doi.org/10.1016/j.colsurfb.2014.02.038.